Symmetry-Breaking Supercollisions in Landau-Quantized Graphene

Florian Wendler, Martin Mittendorff, Jacob C. König-Otto, Samuel Brem, Claire Berger,
Walter A. de Heer, Roman Böttger, Harald Schneider, Manfred Helm, Stephan Winnerl,
and Ermin Malic

Symmetry-breaking supercollisions in Landau-quantized graphene

Florian Wendler,[1, *] Martin Mittendorff,[2, 3] Jacob C. König-Otto,[3, 4] Samuel Brem,[1] Claire Berger,[5, 6] Walter A. de Heer,[5] Roman Böttger,[3] Harald Schneider,[3] Manfred Helm,[3, 4] Stephan Winnerl,[3] and Ermin Malic[7]

[1]*Department of Theoretical Physics, Technical University Berlin, 10623 Berlin, Germany.*
[2]*Institute for Research in Electronics & Applied Physics,*
University of Maryland, College Park, Maryland 20742, United States.
[3]*Helmholtz-Zentrum Dresden-Rossendorf, PO Box 510119, D-01314 Dresden, Germany.*
[4]*Technische Universität Dresden, D-01062 Dresden, Germany.*
[5]*Georgia Institute of Technology, Atlanta, GA 30332, USA*
[6]*Institut Néel, CNRS-Université Alpes, 38042, Grenoble, France*
[7]*Department of Physics, Chalmers University of Technology, 41296 Gothenburg, Sweden.*

Recent pump-probe experiments performed on graphene in a perpendicular magnetic field have revealed carrier relaxation times ranging from picoseconds to nanoseconds depending on the quality of the sample. To explain this surprising behavior, we propose a novel symmetry-breaking defect-assisted relaxation channel. This enables scattering of electrons with single out-of-plane phonons, which drastically accelerate the carrier scattering time in low-quality samples. The gained insights provide a strategy for tuning the carrier relaxation time in graphene and related materials by orders of magnitude.

In graphene, the impact of momentum-conserving acoustic phonon processes on relaxation of non-equilibrium electronic excitations is limited by the low sound velocity, restricting the maximum energy transfer per scattering event [1]. Conversely, defect-assisted electron-phonon scattering events, so called supercollisions, can have a profound impact on the relaxation time by removing the in-plane momentum conservation, since the excess momentum can be absorbed by defects [1–7]. For graphene in a magnetic field, the situation is drastically changed since the in-plane translation symmetry is broken with the consequence that the electron momentum is no longer a conserved quantity, suggesting that supercollisions are not important in Landau-quantized graphene.

In the light of this, the experimental results for electron relaxation times between graphene Landau levels in this letter are very surprising, since they clearly show a strong dependence of the relaxation time on the quality of the sample. To explain these findings, we propose a novel mechanism for defect-assisted electron-phonon scattering breaking the mirror symmetry of the graphene plane. By *defect* we refer to local perturbations introducing additional scattering channels and breaking the mirror symmetry. Such defects could e.g. be local electric field gradients, interstitials, or bucklings of the graphene plane induced by a substrate roughness or by vacancies [8, 9]. In general, the symmetry with respect to a mirror plane lying in the graphene plane prevents the linear coupling of charge carriers and out-of-plane phonons (also known as flexural phonons) in a perfect sample [10, 11]. The removal of the mirror symmetry by defects turns out to be crucial in Landau-quantized graphene, where carrier-phonon scattering is governed by resonances between inter-Landau level transitions and corresponding phonon energies [12, 13]. While the in-plane optical
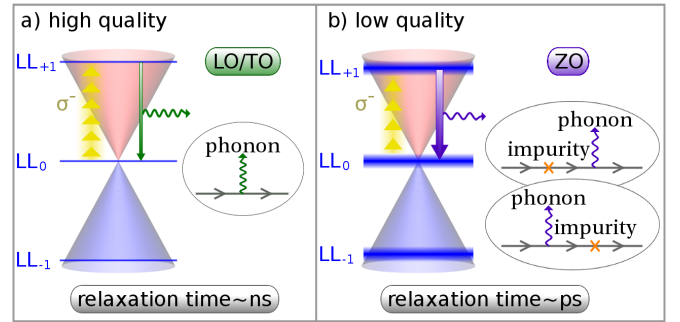

Figure 1. Sketch of (a) carrier-phonon and (b) defect-assisted carrier-phonon scattering channels governing the relaxation in high and low quality samples, respectively. Three broadened Landau levels (LLs) are shown with the Dirac cone in the background. Charge carriers are excited with left circularly polarized radiation (yellow arrows) and relax via scattering with phonons. Feynman diagrams of the scattering processes illustrate the difference between (a) a high quality sample where usual carrier-phonon scattering involving the modes ΓTO, KTO, ΓLO, KLO takes place (green arrows), and (b) a low quality sample where the simultaneous scattering of charge carriers with defects and phonons enable the relaxation via out-of-plane phonons of the mode ΓZO (purple arrows).

phonon energies of graphene range from 150 to 200 meV, the out-of-plane phonon at the Γ point (the ΓZO mode) – activated by defect-electron interaction – has an energy of 100 meV [14–16]. For a sufficiently large Landau level (LL) broadening, supercollisions with ΓZO phonons allow transitions between the three energetically lowest levels $LL_{\pm1}$ and LL_0 at reasonable magnetic fields.

The sketches in Figure 1 compare the ordinary carrier-phonon scattering with the defect-assisted carrier-phonon scattering in two samples with different qualities, where the quality is defined by the concentration of defects breaking the mirror symmetry of the graphene plane.
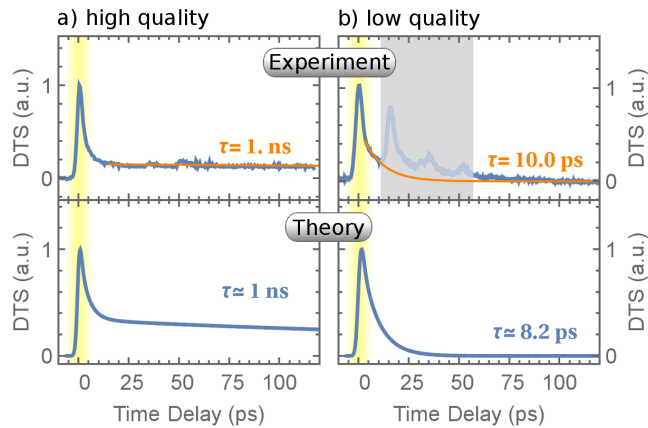
Figure 2. Direct comparison of the carrier relaxation times seen in differential transmission spectra (DTS) of (a) a high quality and (b) a low quality sample in experiment and theory, respectively. This demonstrates that the relaxation time is two orders of magnitude faster in the low quality sample. The yellow area in the background illustrates the width of the pump pulse. The orange signatures show exponential functions fitting the experimental data, and the gray area in the experimental signal indicates secondary peaks appearing due to reflections of the pump pulse which are omitted in our analysis. Experimental DTS for the high quality sample is shown for a longer time range up to 1 ps in the Supplemental Material.

The investigated situation is very similar in both cases: The system is excited using σ^--polarized radiation that is in resonance with the transition $\mathrm{LL}_0 \to \mathrm{LL}_{+1}$, and it develops back to equilibrium via the emission of phonons. While ordinary carrier-phonon scattering (LO/TO) is possible in the high and in the low quality sample, the relaxation in the low quality sample is governed by super-collisions allowing the emission of out-of-plane phonons (ΓZO). The latter phonons have a smaller energy that approximately fits the inter-LL distance of the experiments discussed below. Therefore the relaxation occurs on a picosecond timescale ($\tau \sim 10$ ps) as opposed to a nanosecond timescale ($\tau \sim 1$ ns) in case of a high quality sample.

We present a theoretical study supported by experimental observations. Degenerate pump-probe experiments were carried out on two different multilayer epitaxial graphene samples. To this end, mid-infrared radiation from a free-electron laser (photon energy 75 meV, pulse duration 2.7 ps, pump fluence $0.1\,\mu\mathrm{J/cm^2}$) of σ^--polarization was employed for both pumping and probing. The samples were kept at $10\,\mathrm{K}$ in a magnetic field of $4.2\,\mathrm{T}$ perpendicular to the graphene layers. At this field, both pump and probe beam were resonant with the $\mathrm{LL}_0 \to \mathrm{LL}_{+1}$ transition in the samples. A mercury-cadmium-telluride detector cooled by liquid nitrogen was used for low-noise detection. The two multilayer epitaxial graphene samples were grown by the same technique, namely thermal decomposition of the C-face of semi-insulating 4H-SiC by the confinement controlled sublimation (CCS) method [17], however under slightly different growth conditions. One sample, in the following named "low quality sample" has a low structural quality compared to standard CCS grown epitaxial multilayer graphene. The other one, in the following named "high quality sample" features an extraordinary structural quality with no D-peak in the Raman spectrum [18]. Details on the growth, characterization by Raman spectroscopy and doping of the sample, further pump probe data with and without a magnetic field, details of the theory, and a discussion of the phonon spectrum in multilayer graphene can be found in the Supplemental Material [19].

The applied many-particle theory is based on an expansion of the graphene Bloch equations [20–22] by out-of-plane symmetry-breaking electron-defect interactions. It reproduces well the surprising experimental behavior, where decay times in two samples differ by more than two orders of magnitude, cf. Fig. 2. For the theoretical modeling a pump fluence of $\epsilon_{\mathrm{pf}} = 1 \cdot 10^{-2}\mu\mathrm{J/cm^2}$, and an defect-assisted level broadening of $\Gamma_{\mathrm{de}} = 0.1\mathrm{meV}$ ($\Gamma_{\mathrm{de}} = 10\mathrm{meV}$) is used for the high quality sample (low quality sample). In accordance with Ref. [23], the doping is set to $\mu = 10\,\mathrm{meV}$ in the high quality case, while a value of $\mu = 28\,\mathrm{meV}$ is used in the low quality case as indicated by Ref. [24]. Before the relaxation processes dominate, i.e. during the excitation pulse, peaks in the transmission featuring very fast decay times occur. They result from the optical excitation as well as Auger scattering. Since those have already been discussed in Ref. [24], we focus on the slower relaxation in this work. While the high quality sample exhibits a very slow relaxation time of about $\tau \sim 1\,\mathrm{ns}$, the relaxation is much faster in case of the low quality sample reaching times in the range of $\tau \sim 10\,\mathrm{ps}$.

The explanation for the strong dependence of the relaxation time on the sample quality is two-fold: First, as was already mentioned above, the carrier-phonon relaxation rate in Landau-quantized graphene is determined by a resonance condition of phonon energy and the energy of the inter-LL transition. If both energies coincide for a specific inter-LL transition, carrier-phonon scattering is efficient between the two involved LLs. Second, the exact resonance condition is weakened by a finite broadening that is given by the dephasing of Landau transitions which also determines the LL broadening [25]. Therefore, off-resonant scattering is possible and its efficiency increases with the broadening of the Landau levels. Consequently, the relaxation is faster in low quality samples where the Landau level broadening is larger. The resonance condition is determined by the magnetic field, responsible for the formation of Landau-states. For the LL-transition in a range of $100\,\mathrm{meV}$, investigated here, only flexural phonons (ΓZO) provide a fitting energy channel. However, the corresponding electron-phonon scattering is symmetry

forbidden in pure graphene [10]. Here, we propose that this relaxation channel is activated in low quality samples of Landau-quantized graphene by enabling carrier-flexural phonon (ΓZO) scattering due to defect-assisted electron-phonon scattering. Only if both factors (a sufficient LL-broadening and the activation of flexural phonons) are taken into account, the experimentally observed dependence of the relaxation time on the quality of the sample can be explained.

We proceed to set forth the details of the theory of symmetry-breaking supercollisions in Landau-quantized graphene to explain the microscopic background of the observed surprising sample-dependent relaxation behavior. The defect-assisted carrier-phonon scattering is described by the Hamiltonian $H = H_0 + H_{\text{el-de}} + H_{\text{el-ph}}$, consisting of a free energy part $H_0 = \sum_i \epsilon_i a_i^\dagger a_i + \sum_{\mathbf{p},\mu} \epsilon_{\mu\mathbf{q}_{\text{ph}}} \left(b_{\mu\mathbf{q}_{\text{ph}}}^\dagger b_{\mu\mathbf{q}_{\text{ph}}} + 1/2 \right)$ and two perturbations stemming from disorder $H_{\text{el-de}} = \sum_{i,f} D_{i,f} a_f^\dagger a_i$ and the electron-phonon coupling $H_{\text{el-ph}} = \sum_{i,f} \sum_{\mu\mathbf{q}_{\text{ph}}} g_{i,f}^{\mu,\mathbf{q}_{\text{ph}}} a_f^\dagger a_i \left(b_{\mu,\mathbf{q}_{\text{ph}}} + b_{\mu,-\mathbf{q}_{\text{ph}}}^\dagger \right)$. Here, and in the remainder of this article, the electronic states are specified by a compound index i comprising the spin $s_i = \pm 1$, valley $\xi_i = \pm 1$, band $\lambda_i = \pm 1$, Landau level index $n_i = 0, 1, 2, \ldots$, and the quantum number $m_i = 0, 1, 2, \ldots N_B - 1$ giving rise to the large LL degeneracy $N_B = AeB/(2\pi\hbar)$ that scales linearly with the area of graphene A, the elementary charge e and the magnetic field strength B. Neglecting the Zeeman effect and the spin-orbit interaction, both of which are small as compared to the level broadening in graphene [26], the low-energetic Landau level spectrum is given by $\epsilon_i = \lambda_i v_{\text{F}} \sqrt{2 n_i \hbar e B}$, with the Fermi velocity [27] $v_{\text{F}} \approx 1\,\text{nm/fs}$. Furthermore, optical phonons are characterized by their mode μ, momentum $\hbar\mathbf{q}_{\text{ph}}$ and energy $\epsilon_{\mu\mathbf{q}_{\text{ph}}} \approx \epsilon_\mu$, and the matrix elements $D_{i,f}$ and $g_{i,f}^{\mu,\mathbf{q}_{\text{ph}}}$ determine the probabilities of the transition from the initial to the final electronic states $|i\rangle \to |f\rangle$ due to electron-defect and electron-phonon scattering, respectively.

Starting from the Hamiltonian above, the supercollision matrix element is obtained by a multiple scattering expansion [28] to the lowest necessary order in the LL-basis (Fig. 1b, inset)

$$\widetilde{g}_{i,f} = \langle f| \left[H_{\text{el-de}} G_0^\dagger(\epsilon_f) H_{\text{el-ph}} + H_{\text{el-ph}} G_0(\epsilon_i) H_{\text{el-de}} \right] |i\rangle. \tag{1}$$

Introducing a finite broadening Γ, the free electron Green's function reads $G_0(E) = (E - H_0 + i\Gamma)^{-1}$, which yields the supercollision matrix element

$$\left. \widetilde{g}_{i,f}^{\mu,\mathbf{q}_{\text{ph}}} \right|^{\text{em/ab}} \simeq \sum_v \left[g_{i,v}^{\mu,\mp\mathbf{q}_{\text{ph}}} \frac{1}{\epsilon_i - \epsilon_v \mp \epsilon_{\mu,\mathbf{q}_{\text{ph}}} + i\Gamma} D_{v,f} \right.$$
$$\left. + D_{i,v} \frac{1}{\epsilon_i - \epsilon_v + i\Gamma} g_{v,f}^{\mu,\mp\mathbf{q}_{\text{ph}}} \right], \tag{2}$$

for the emission $(-)$ and absorption $(+)$ of the phonon $(\mu, \mathbf{q}_{\text{ph}})$. In the regime of well-separated Landau levels, we set $D_{i,f} \to D_{i,f} \delta_{\lambda_i,\lambda_f} \delta_{n_i,n_f}$, so that the denominator of the second term in Eq. (2) reduces to $i\Gamma$. In a self-consistent Born-Markov approximation, the parameter Γ is identified by the quantum mechanical dephasing $\Gamma_{i,f}$ which determines the LL-broadening [25] and will be explained below. The discussion of the pure LL-defect and the pure LL-phonon interaction can be found in the Supplemental Material.

Using the supercollision matrix element from Eq. 2, we calculate the transition probability for the emission and absorption of phonons using the generalized Fermi's golden rule [29]

$$W_{i,f} = \frac{2\pi}{\hbar} \sum_{\mu,\mathbf{q}_{\text{ph}}} \left| \widetilde{g}_{i,f}^{\mu,\mathbf{q}_{\text{ph}}} \right|^2 \tag{3}$$
$$\left[(n_\mu + 1) L_{\Gamma_{if}} \left(\triangle E_{i,f,\mu}^{\text{em}} \right) + n_\mu L_{\Gamma_{if}} \left(\triangle E_{i,f,\mu}^{\text{ab}} \right) \right],$$

with the energy differences $\triangle E_{i,f,\mu}^{\text{em/ab}} = \epsilon_i - \epsilon_f \mp \epsilon_\mu$ for the emission $(-)$ and absorption $(+)$ of a phonon, the Bose distribution n_μ, and the Lorentzian $L_\Gamma(\triangle E) = \Gamma/\left(\pi \left(\triangle E^2 + \Gamma^2 \right) \right)$ expressing energy conservation. Then, the carrier dynamics becomes accessible via the graphene Bloch equations [20, 22]

$$\dot{\rho}_i = \sum_j \left[W_{j,i} \rho_j \left(1 - \rho_i \right) - W_{i,j} \rho_i \left(1 - \rho_j \right) \right], \tag{4}$$

$$\dot{p}_{i,f} = -\frac{\Gamma_{i,f}}{\hbar} p_{i,f}, \tag{5}$$

for the occupation probability $\rho_i(t) = \langle a_i^\dagger a_i \rangle(t)$ and the microscopic polarization $p_{i,f}(t) = \langle a_f^\dagger a_i \rangle(t)$, where Eq. 4 is equivalent to the Boltzmann equation. The electron-light, electron-electron and ordinary electron-phonon interactions are omitted for reasons of clarity. Their contribution to the carrier dynamics is taken into account in the numerical evaluation, but it has been explained elsewhere [22, 24, 30]. The total dephasing rate $\Gamma_{i,f} = \Gamma_{i,f}^{\text{de}} + \Gamma_{i,f}^{\text{el-el}} + \Gamma_{i,f}^{\text{el-ph}} + \Gamma_{i,f}^{\text{el-de-ph}}$ determines the broadening of the LLs and is composed of the defect-induced dephasing $\Gamma_{i,f}^{\text{de}}$, and the dephasing contributions due to the different many-particle scattering channels. For details about $\Gamma_{i,f}^{\text{de}}$, $\Gamma_{i,f}^{\text{el-el}}$ and $\Gamma_{i,f}^{\text{el-ph}}$ we refer to Ref. [25]. The dephasing induced by supercollisions is given by

$$\Gamma_{i,f}^{\text{el-de-ph}} = \sum_j \left[(W_{j,i} + W_{j,f}) \rho_j + (W_{i,j} + W_{f,j})(1 - \rho_j) \right]. \tag{6}$$

Note that the scattering rates given by Eq. 3 depend on the total dephasing $\Gamma_{i,f}$ which is needed to calculate the dephasing due to supercollisions. Therefore, the total dephasing is calculated self-consistently in every time step of the numerical evaluation of the Bloch equations (Eqs. 4-5) [31].
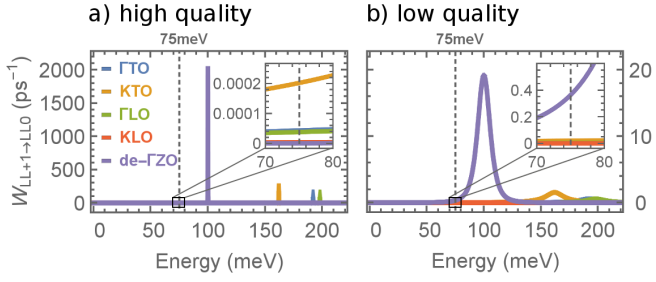
Figure 3. Scattering rates induced by different phonon modes in dependence of the inter-LL transition energy showing clear electron-phonon resonance peaks for (a) the high quality ($\Gamma_{\mathrm{de}} = 0.1\,$meV) and (b) the low quality sample ($\Gamma_{\mathrm{de}} = 10\,$meV). At a magnetic field of $B = 4.2\,$T (used in the experiments), the relevant inter-LL spacings are $75\,$meV (dotted vertical lines). The insets show that in this energy range defect-assisted electron-ΓZO-phonon scattering (de-ΓZO) clearly dominates in the low quality sample, while it is negligible in the high quality sample.

Figure 4. (a) Relaxation time as a function of the defect-induced dephasing for different dopings μ. The dashed vertical lines mark the values of the defect-induced dephasing that were used to model the high quality ($\Gamma_{\mathrm{de}} = 0.1\,$meV) and the low quality ($\Gamma_{\mathrm{de}} = 10\,$meV) samples. (b) Initial occupation probability of LL_0 in dependence of the doping of the sample, and effective doping for a magnetic field of $B = 4.2\,$T assuming that the carrier density does not change when the magnetic field is turned on. The dashed vertical lines mark the values of the doping that are used in (a).

Before we examine the numerical results in more detail, we investigate how the scattering rates scale with the defect-induced dephasing. In case of highly off-resonant electron-phonon scattering ($\Gamma_{i,f} \ll \Delta E$), the absolute square of the supercollision matrix element (Eq. 2) scales like $|\widetilde{g}_{i,f}^{\mu, \mathbf{q}_{\mathrm{ph}}}|^2 \propto \Gamma_{\mathrm{de}}^2/\Gamma_{i,f}^2$, the Lorentzians in the scattering rate (Eq. 3) can be approximated as $\pi L_{\Gamma_{i,f}}(\Delta E) \simeq \Gamma_{i,f}/\Delta E^2$, and the scattering rate hence scales like $W_{i,f} \propto \Gamma_{\mathrm{de}}^2/\Gamma_{i,j}$. Moreover, in this off-resonant regime, the self-consistently determined dephasing $\Gamma_{i,f}$ is generally of the same order of magnitude as the defect-induced dephasing $\Gamma_{i,f}^{\mathrm{de}}$, which yields an effective linear scaling of $W_{i,f}$ with $\Gamma_{i,f}^{\mathrm{de}}$. Consequently, to approximate the scattering rate $W_{LL+1 \to LL_0}$ for supercollisions as well as the other relevant electron-phonon scattering channels, we set $\Gamma_{i,f} \to \Gamma_{i,f}^{\mathrm{de}}$. The result is shown in Fig. 3 and demonstrates that normal electron-phonon scattering is suppressed mainly due to the high optical phonon energies, and likewise the smaller energy of the ΓZO-mode explains its importance for the relaxation in Landau-quantized graphene. In the regime of well-separated Landau levels, on the other hand, the energy of acoustic phonons is too small to have an impact on the carrier dynamics, cf. Ref [22]. Furthermore, Fig. 3 shows that, in the high quality sample, the supercollisions are strongly suppressed in the relevant (off-resonant) energy range, cf. inset of Fig. 3a, since the off-resonance enters not only through the Lorentzian broadening in Eq. 3 (like in the case of ordinary electron-phonon scattering) but also through the energy differences in the supercollision matrix element (Eq. 2). In the low quality sample, on the other hand, the total dephasing is so large that the relevant energy lies within the broadened resonance peak of the supercollisions (purple line in Fig. 3b), which is thus the dominant relaxat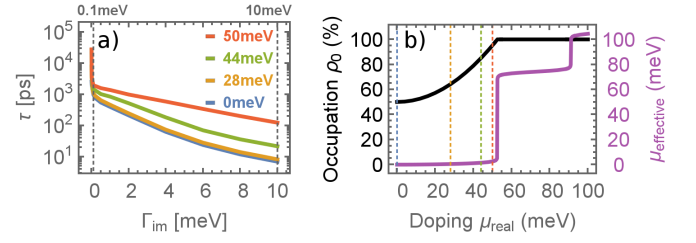ion channel in this case. Therefore, the sample quality determining the total dephasing (via $\Gamma_{i,f}^{\mathrm{de}}$), critically influences the relaxation. This is the key to understand the drastic difference in the relaxation times of the two experimentally investigated graphene samples, cf. Fig. 2. Note that the peak heights in Fig. 3 are not to be trusted, since the scattering rates shown in Fig. 3 are only valid in the off-resonant regime ($\Gamma_{i,f} \ll \Delta E$).

The dependence of the relaxation time on the defect-induced dephasing, which is a measure for the sample quality, is shown in Fig. 4 (a) for different values of the doping. It shows a very slow relaxation for samples with zero disorder $\tau \sim 10\,$ns which becomes about three orders of magnitude faster as the disorder concentration is increased. The very strong decrease of τ for vanishing defect-induced dephasings $\Gamma_{\mathrm{de}} < 0.1\,$meV occurs due to the fact, that in this case the defect-induced dephasing is no longer the dominant contribution to the total dephasing Γ. Instead, in the regime $\Gamma_{\mathrm{de}} \ll \Gamma$, the total dephasing is essentially determined by electron-electron scattering that does not change the occupations – known as pure-dephasing –, but constitutes a scattering channel which competes with relaxation channels (like electron-phonon scattering and supercollisions). Furthermore, we observe that the relaxation time depends on the doping of the sample, since this determines the initial occupations and therewith the Pauli blocking, cf. the occupations in Eq. 4. Considering solely the transition $LL_{+1} \to LL_0$, Eq. 4 reads $\dot{\rho}_{+1} = -W_{+1 \to 0}\rho_{+1}(1 - \rho_0)$, which – assuming a constant ρ_0 – yields an exponential decay $\rho_{+1} = \exp(-t/\tau)$ with the relaxation time $\tau = 1/(W_{+1 \to 0}(1 - \rho_0))$. This illustrates that τ can become very large for a nearly completely filled LL_0. To understand the minimal change of the relaxation time for dopings below $\sim 28\,$meV and the marked change for higher dopings, we take a look at the initial value of the occupation ρ_0 in dependence of the doping of the sample, cf. black line in Fig. 4 (b), resulting from a Fermi distribution for an effective doping (purple

line). The effective doping $\mu_{\text{effective}}$ for a magnetic field of $B = 4.2\,\text{T}$ is calculated from the doping in the absence of a field μ_{real} using the criterion that the carrier density does not change when the magnetic field is switched on, cf. Ref. [24]. The observation that LL_0 is far from being completely filled for low dopings, while it is almost filled for dopings higher than $\mu_{\text{real}} \sim 40\,\text{meV}$, explains the doping dependence of the relaxation time.

Finally, we compare the obtained results to magneto-transport experiments from Refs. 32 and 33, where the temperature dependence of energy loss rates in a variety of Landau-quantized graphene samples was measured. The results are in agreement with ordinary supercollisions involving acoustic phonons, and the high-field energy loss rates are only about 40 % smaller in comparison to the zero-field case. This seems to contradict our results but in fact it is consistent with our interpretation. The samples used in the aforementioned magnetotransport experiments are single layer graphene samples with a finite doping, where the Fermi energy lies at the 8th Landau level or higher. Therefore, according to the findings of Ref. 34, the experiments are performed in a regime where the Landau levels are not well separated, i.e. adjacent Landau levels overlap. Consequently, scattering with low energetic acoustic phonons and ordinary supercollisions have a profound impact on the relaxation dynamics, but supercollisions do no dramatically change the carrier dynamics. On the other hand, the present paper studies one particular inter-Landau level transition ($\text{LL}_0 \rightarrow \text{LL}_{+1}$), where an energy gap of a few tens of meV efficiently suppresses acoustic phonon scattering (too low energy) and also in-plane optical phonon scattering (too high energy). Here, the activation of the ΓZO phonon mode having an intermediate energy can lead to a dramatically different relaxation dynamics.

In summary, the relaxation time in Landau-quantized graphene shows a very distinct dependence on the sample quality. This is explained by a novel defect-assisted electron-phonon scattering channel, in which disorder breaks the mirror symmetry of graphene. These findings demonstrate that varying the amount of disorder can be used to tailor the relaxation time in this system over several orders of magnitude.

* florian.wendler@fu-berlin.de

[1] J. C. W. Song, M. Y. Reizer, and L. S. Levitov, Phys. Rev. Lett. **109**, 106602 (2012).

[2] M. W. Graham, S.-F. Shi, D. C. Ralph, J. Park, and P. L. McEuen, Nat. Phys. **9**, 103 (2013).

[3] A. C. Betz, S. H. Jhang, E. Pallecchi, R. Ferreira, G. Feve, J.-M. Berroir, and B. Placais, Nat. Phys. **9**, 109 (2013).

[4] M. W. Graham, S.-F. Shi, Z. Wang, D. C. Ralph, J. Park, and P. L. McEuen, Nano Lett. **13**, 5497 (2013), pMID: 24124889.

[5] V. Eless, T. Yager, S. Spasov, S. Lara-Avila, R. Yakimova, S. Kubatkin, T. J. B. M. Janssen, A. Tzalenchuk, and V. Antonov, Appl. Phys. Lett. **103**, 093103 (2013), http://dx.doi.org/10.1063/1.4819726.

[6] A. Laitinen, M. Oksanen, A. Fay, D. Cox, M. Tomi, P. Virtanen, and P. J. Hakonen, Nano Lett. **14**, 3009 (2014), pMID: 24842236.

[7] T. V. Alencar, M. G. Silva, L. M. Malard, and A. M. de Paula, Nano Lett. **14**, 5621 (2014), pMID: 25211670, http://dx.doi.org/10.1021/nl502163d.

[8] R. H. Telling, C. P. Ewels, A. A. El-Barbary, and M. I. Heggie, Nat. Mater. **2**, 333 (2003).

[9] F. Banhart, J. Kotakoski, and A. V. Krasheninnikov, *ACS Nano*, ACS Nano **5**, 26 (2011).

[10] E. Mariani and F. von Oppen, Phys. Rev. Lett. **100**, 076801 (2008).

[11] E. Mariani and F. von Oppen, Phys. Rev. B **82**, 195403 (2010).

[12] F. Wendler, A. Knorr, and E. Malic, Appl. Phys. Lett. **103**, 253117 (2013).

[13] F. Wendler and E. Malic, Phys. Status Solidi B **251**, 2541 (2014).

[14] J. Maultzsch, S. Reich, C. Thomsen, H. Requardt, and P. Ordejón, Phys. Rev. Lett. **92**, 075501 (2004).

[15] E. Malic, T. Winzer, E. Bobkin, and A. Knorr, Phys. Rev. B **84**, 205406 (2011).

[16] A. Politano, F. de Juan, G. Chiarello, and H. A. Fertig, Phys. Rev. Lett. **115**, 075504 (2015).

[17] W. A. de Heer, C. Berger, M. Ruan, M. Sprinkle, X. Li, Y. Hu, B. Zhang, J. Hankinson, and E. Conrada, Proc. Nat. Acad. Sci. **108**, 16900 (2011).

[18] W. A. de Heer, C. Berger, X. Wu, M. Sprinkle, Y. Hu, M. Ruan, J. A. Stroscio, P. N. First, R. Haddon, B. Piot, C. Faugeras, M. Potemski, and J.-S. Moon, J. Phys. D: Appl. Phys. **43**, 374007 (2010).

[19] See Supplemental Material [url] for experimental and theoretical details, which includes Refs. 35–49.

[20] E. Malic and A. Knorr, *Graphene and Carbon Nanotubes: Ultrafast Optics and Relaxation Dynamics* (Wiley-VCH, 2013).

[21] H. Haug and S. W. Koch, *Quantum Theory of the Optical and Electronic Properties of Semiconductors* (World Scientific, 2009).

[22] F. Wendler, A. Knorr, and E. Malic, Nanophotonics **4**, 224 (2015).

[23] R. J. Suess, S. Winnerl, H. Schneider, M. Helm, C. Berger, W. A. de Heer, T. E. Murphy, and M. Mittendorff, *ACS Photonics*, ACS Photonics **3**, 1069 (2016).

[24] M. Mittendorff, F. Wendler, E. Malic, A. Knorr, M. Orlita, M. Potemski, C. Berger, W. A. de Heer, H. Schneider, M. Helm, and S. Winnerl, Nature Phys. **11**, 75 (2015).

[25] H. Funk, A. Knorr, F. Wendler, and E. Malic, Phys. Rev. B **92**, 205428 (2015).

[26] M. O. Goerbig, Rev. Mod. Phys. **83**, 1193 (2011).

[27] A. H. Castro Neto, F. Guinea, N. M. R. Peres, K. S. Novoselov, and A. K. Geim, Rev. Mod. Phys. **81**, 109 (2009).

[28] E. N. Economou, *Green's Functions in Quantum Physics* (Springer Berlin Heidelberg, 2006).

[29] H. Bruus and K. Flensberg, *Many-Body Quantum Theory in Condensed Matter Physics* (Oxford University Press, 2009).

[30] F. Wendler, A. Knorr, and E. Malic, Nature Commun. **5**, 3703 (2014).

[31] To this end, starting with an initial dephasing $\Gamma_{i,f}|^0$, a sequence of dephasings $\Gamma_{i,f}|^1$, $\Gamma_{i,f}|^2$, ... is calculated where the preceding dephasing $\Gamma_{i,f}|^{l-1}$ is used to calculate the dephasing $\Gamma_{i,f}|^l$, respectively, until two consecutive dephasings are equal.

[32] A. M. R. Baker, J. A. Alexander-Webber, T. Altebaeumer, and R. J. Nicholas, Phys. Rev. B **85**, 115403 (2012).

[33] A. M. R. Baker, J. A. Alexander-Webber, T. Altebaeumer, S. D. McMullan, T. J. B. M. Janssen, A. Tzalenchuk, S. Lara-Avila, S. Kubatkin, R. Yakimova, C.-T. Lin, L.-J. Li, and R. J. Nicholas, Phys. Rev. B **87**, 045414 (2013).

[34] M. Orlita, C. Faugeras, R. Grill, A. Wysmolek, W. Strupinski, C. Berger, W. A. de Heer, G. Martinez, and M. Potemski, Phys. Rev. Lett. **107**, 216603 (2011).

[35] D. Sun, Z.-K. Wu, C. Divin, X. Li, C. Berger, W. A. de Heer, P. N. First, and T. B. Norris, Phys. Rev. Lett. **101**, 157402 (2008).

[36] M. Orlita, C. Faugeras, P. Plochocka, P. Neugebauer, G. Martinez, D. K. Maude, A.-L. Barra, M. Sprinkle, C. Berger, W. A. de Heer, and M. Potemski, Phys. Rev. Lett. **101**, 267601 (2008).

[37] J. C. König-Otto, M. Mittendorff, T. Winzer, F. Kadi, E. Malic, A. Knorr, C. Berger, W. A. de Heer, A. Pashkin, H. Schneider, M. Helm, and S. Winnerl, Phys. Rev. Lett. **117**, 087401 (2016).

[38] C. Faugeras, A. Nerrière, M. Potemski, A. Mahmood, E. Dujardin, C. Berger, and W. A. de Heer, Appl. Phys. Lett. **92**, 011914 (2008), http://aip.scitation.org/doi/pdf/10.1063/1.2828975.

[39] S. Berciaud, S. Ryu, L. E. Brus, and T. F. Heinz, Nano Lett. **9**, 346 (2009).

[40] D. S. Lee, C. Riedl, B. Krauss, K. von Klitzing, U. Starke, and J. H. Smet, Nano Lett. **8**, 4320 (2008).

[41] J. M. Dawlaty, S. Shivaraman, M. Chandrashekhar, F. Rana, and M. G. Spencer, Appl. Phys. Lett. **92**, 042116 (2008).

[42] S. Winnerl, M. Orlita, P. Plochocka, P. Kossacki, M. Potemski, T. Winzer, E. Malic, A. Knorr, M. Sprinkle, C. Berger, W. A. de Heer, H. Schneider, and M. Helm, Phys. Rev. Lett. **107**, 237401 (2011).

[43] M. T. Mihnev, F. Kadi, C. J. Divin, T. Winzer, S. Lee, C.-H. Liu, Z. Zhong, C. Berger, W. a. de Heer, E. Malic, A. Knorr, and T. B. Norris, Nat. Commun. **7**, 11617 (2016).

[44] O. Lehtinen, J. Kotakoski, A. V. Krasheninnikov, A. Tolvanen, K. Nordlund, and J. Keinonen, Phys. Rev. B **81**, 153401 (2010).

[45] E. H. Åhlgren, J. Kotakoski, and A. V. Krasheninnikov, Phys. Rev. B **83**, 115424 (2011).

[46] E. Akkermans and G. Montambaux, *Mesoscopic Physics of Electrons and Photons* (Cambridge University Press, 2007).

[47] D. M. Basko, S. Piscanec, and A. C. Ferrari, Phys. Rev. B **80**, 165413 (2009).

[48] A. I. Cocemasov, D. L. Nika, and A. A. Balandin, Phys. Rev. B **88**, 035428 (2013).

[49] J. Hass, F. Varchon, J. E. Millán-Otoya, M. Sprinkle, N. Sharma, W. A. de Heer, C. Berger, P. N. First, L. Magaud, and E. H. Conrad, Phys. Rev. Lett. **100**, 125504 (2008).